The Astrophysical Journal, 979:7 (17pp), 2025 January 20 https://doi.org/10.3847/1538-4357/ad94ef

The Effect of Galaxy Interactions on Starbursts in Milky Way-mass Galaxies in FIRE Simulations

Fei Li (李菲)[1,2], Mubdi Rahman[3], Norman Murray[2,4], Dušan Kereš[5], Andrew Wetzel[6], Claude-André Faucher-Giguère[7], Philip F. Hopkins[8], and Jorge Moreno[9,10]
[1] David A. Dunlap Department of Astronomy and Astrophysics, University of Toronto, 50 Saint George Street, ON M5S 3H4, Canada; lif.li@mail.utoronto.ca
[2] Canadian Institute for Theoretical Astrophysics, University of Toronto, 60 Saint George Street, Toronto, ON M5S 3H8, Canada
[3] Sidrat Research, 124 Merton Street, Suite 507, Toronto, ON M4S 2Z2, Canada
[4] Canada Research Chair in Astrophysics, Canada
[5] Department of Physics, Center for Astrophysics and Space Sciences, University of California at San Diego, 9500 Gilman Drive, La Jolla, CA 92093, USA
[6] Department of Physics & Astronomy, University of California, Davis, CA 95616, USA
[7] Department of Physics and Astronomy and CIERA, Northwestern University, 2145 Sheridan Road, Evanston, IL 60208, USA
[8] TAPIR, Mailcode 350-17, California Institute of Technology, Pasadena, CA 91125, USA
[9] Department of Physics and Astronomy, Pomona College, Claremont, CA 91711, USA
[10] The Observatories of the Carnegie Institution for Science, 813 Santa Barbara Street, Pasadena, CA 91101, USA
Received 2024 August 9; revised 2024 November 15; accepted 2024 November 18; published 2025 January 13

Abstract

Simulations and observations suggest that galaxy interactions may enhance the star formation rate (SFR) in merging galaxies. One proposed mechanism is the torque exerted on the gas and stars in the larger galaxy by the smaller galaxy. We analyze the interaction torques and star formation activity on six galaxies from the FIRE-2 simulation suite with masses comparable to the Milky Way galaxy at redshift $z = 0$. We trace the halos from $z = 3.6$ to $z = 0$, calculating the torque exerted by the nearby galaxies on the gas in the central galaxy. We calculate the correlation between the torque and the SFR across the simulations for various mass ratios. For near-equal-stellar-mass-ratio interactions in the galaxy sample, occurring between $z = 1.2-3.6$, there is a positive and statistically significant correlation between the torque from nearby galaxies on the gas of the central galaxies and the SFR. For all other samples, no statistically significant correlation is found between the torque and the SFR. Our analysis shows that some, but not all, major interactions cause starbursts in the simulated Milky Way-mass galaxies, and that most starbursts are not caused by galaxy interactions. The transition from "bursty" at high redshift ($z \gtrsim 1$) to "steady" star formation state at later times is independent of the interaction history of the galaxies, and most of the interactions do not leave significant imprints on the overall trend of the star formation history of the galaxies.

Unified Astronomy Thesaurus concepts: Galaxy evolution (594); Galaxy interactions (600)

1. Introduction

Simulations of galaxies that resolve the interstellar medium (ISM) at giant molecular cloud-scales show that massive galaxies transition from a "bursty" star formation state with large temporal fluctuations in star formation rate (SFR) at high redshift to a "steady" star formation state at low redshift (P. F. Hopkins et al. 2014, 2018; A. L. Muratov et al. 2015; M. Sparre et al. 2017; C.-A. Faucher-Giguère 2018). It is worth noting that this connects broadly with the transition from a thick to thin disk geometry (S. Yu et al. 2021, 2023; F. McCluskey et al. 2024). The physical cause of this transition, however, remains uncertain (J. Stern et al. 2021; A. B. Gurvich et al. 2023; P. F. Hopkins et al. 2023). A proposed mechanism is the change in merger and flyby frequency with redshift (J. E. Barnes & L. Hernquist 1996). In this paper, we investigate this mechanism by looking at the effects of galaxy interactions on the star formation activity of central galaxies and their likelihood to trigger starburst events.

Mergers and flybys (J. Moreno 2012; J. Moreno et al. 2013) are common in the growth history of galaxies in the ΛCDM cosmological model, and it is commonly believed that galaxy interactions can induce star formation in central galaxies. Previous simulations have shown that the torque from a companion galaxy exerted on the central galaxy can lead to the inflow of gas, and thus to the enhancement of the SFR in the central galaxy (A. Toomre & J. Toomre 1972; W. C. Keel et al. 1985; D. B. Sanders et al. 1988; J. E. Barnes & L. Hernquist 1996; J. C. Mihos & L. Hernquist 1996; P. B. Tissera et al. 2002; T. J. Cox et al. 2006; M. Montuori et al. 2010; D. S. N. Rupke et al. 2010; P. Torrey et al. 2012). Consistent with the insight from the simulations, there have also been observations (R. B. Larson & B. M. Tinsley 1978; E. J. Barton et al. 2000, 2007; M. S. Alonso et al. 2004; B. Nikolic et al. 2004; D. F. Woods et al. 2006, 2010; D. F. Woods & M. J. Geller 2007; S. L. Ellison et al. 2008, 2010; A. Heiderman et al. 2009; J. H. Knapen & P. A. James 2009; A. R. Robaina et al. 2009; D. R. Patton et al. 2011) showing that near redshift zero the presence of nearby galaxies coincides with higher SFR and that the separation of companions is inversely correlated with the SFR.

Compared to galaxies in the star-forming main sequence, a larger fraction of starburst galaxies displays merger features (W. Luo et al. 2014; J. H. Knapen & M. Cisternas 2015; K. A. Blumenthal et al. 2020). In observations of the local universe, the majority of ultraluminous infrared galaxies ($L_{\rm IR} \geqslant 10^{12} L_{\odot}$, i.e., extreme starbursts) display features of strongly interacting systems, such as bridges, tidal tails, and

disturbed morphologies (e.g., S. Veilleux et al. 2002; Y. Gao & P. M. Solomon 2004; L. Colina et al. 2005; S. García-Burillo et al. 2012; C.-L. Hung et al. 2013).

At higher redshift, mergers are more common. In addition, if the impact of mergers on the SFR activity is similar to the local universe, it is reasonable to assume that a larger fraction of the stellar mass created in that epoch is directly attributable to mergers. However, whether the effect of galaxy interactions on SFR enhancement at high redshift is different from the local universe is unclear. Some observational studies (G. Rodighiero et al. 2011; C. Schreiber et al. 2015; E. K. Lofthouse et al. 2017; A. Silva et al. 2018; W. J. Pearson et al. 2019) show a measurable but marginally statistically significant enhancement of the SFR in merging galaxies compared to the nonmerging sample. There are simulations of idealized galaxies (V. Perret et al. 2014; J. M. Scudder et al. 2015; J. Fensch et al. 2017) with gas fractions typical of high-redshift galaxies, which found that the merger-induced star formation enhancement is weaker compared to galaxies with lower gas fractions.

The tidal features of galaxy interactions with lower mass ratios are more difficult to observe (especially at high redshift) due to lower surface brightness, and minor interactions (stellar mass ratios $\mu \leqslant 0.25$; R. A. Jackson et al. 2022) and mini-interactions ($\mu \leqslant 0.1$; C. Bottrell et al. 2024) have been difficult to observe, but new facilities may improve this situation. Galaxy simulations that can predict the observable properties can be useful in studying the effect of galaxy interactions of various mass ratios on the star formation history.

The FIRE[11] suite of simulations (P. F. Hopkins et al. 2014, 2018) provide a useful laboratory to investigate how interactions affect the internal star formation properties of a galaxy. These simulations explicitly model the radiation pressure, stellar winds, and ionization of young stellar populations to account for the effects of feedback from star formation on their natal environment. This provides a physically realistic model of star formation that has shown success in reproducing a diverse range of observational results, from the relationship between stellar mass and halo mass of galaxies (P. F. Hopkins et al. 2014, 2018; R. Feldmann et al. 2017) to the mass–metallicity relationship of stars and gas within galaxies (X. Ma et al. 2016; A. R. Wetzel et al. 2016; L. Bassini et al. 2024; A. Marszewski et al. 2024). A defining feature of star formation in FIRE is its burstiness, which has been noted as key to how these simulations may be able to reproduce a variety of observational properties (A. L. Muratov et al. 2015; M. Sparre & V. Springel 2016; X. Ma et al. 2017; J. Stern et al. 2021; S. Yu et al. 2021, 2023; A. B. Gurvich et al. 2023; G. Sun et al. 2023).

In this paper, we study the effect of tidal interactions on the star formation activity of the central galaxy using six zoom-in simulations of Milky Way-mass star-forming galaxies from the FIRE-2 simulation suite (P. F. Hopkins et al. 2018). In particular, we analyze the effects of major interactions (stellar mass ratios $\mu \geqslant 0.25$), minor interactions ($0.1 \leqslant \mu < 0.25$), and mini-interactions ($0.01 \leqslant \mu < 0.1$) on the star formation histories of the central galaxies. The major interactions in our sample occur at high redshifts, between $z = 1.2$ and $z = 3.6$.

The outline of this paper is as follows. In Section 2, we describe the simulations used in the analysis, the halo tracing methods, the SFR calculation and detrending, the classification of galaxy interactions, and the torque calculation. In Section 3, we show the results of this study. In Section 4, we discuss the results. Finally, in Section 5 we summarize the main findings from this study.

We adopt a standard flat ΛCDM cosmology with cosmological parameters $H_0 = 70.2\,\mathrm{km\,s^{-1}\,Mpc^{-1}}$, $\Omega_\Lambda = 0.728$, $\Omega_m = 1 - \Omega_\Lambda = 0.272$, $\Omega_b = 0.0455$, $\sigma_8 = 0.807$, and $n = 0.961$.

Table 1
Simulated Galaxies in This Study and their Parameters

Name	$M^0_{\rm halo}$ ($10^{12}\,M_\odot$)	$M^0_\star$ ($10^{10}\,M_\odot$)	$R^0_{\rm vir}$ (kpc)	$m_{\rm dm}$ ($M_\odot$)	References
m12w	1.08	5.7	301	39,000	(1)
m12i	1.18	6.3	311	35,000	(2)
m12c	1.35	5.8	328	35,000	(3)
m12b	1.43	8.5	331	35,000	(3)
m12m	1.58	11	341	35,000	(4)
m12f	1.71	7.9	352	35,000	(5)

Note. Columns: (1) Name: Simulation designation (2) $M^0_{\rm halo}$: Approximate mass of the $z = 0$ main halo (most massive halo in the high-resolution region). (3) $M^0_\star$: Stellar mass of the central galaxy in the main halo at $z = 0$. (4) $R^0_{\rm vir}$: $R_{\rm vir}$ of the $z = 0$ main halo as identified through the Rockstar Halo Finder, which corresponds to R_{360} (P. S. Behroozi et al. 2013a). (5) $m_{\rm dm}$: Dark matter particle mass (6) References: (1): J. Samuel et al. (2020), (2): A. R. Wetzel et al. (2016), (3): S. Garrison-Kimmel et al. (2019), (4): P. F. Hopkins et al. (2018), and (5): S. Garrison-Kimmel et al. (2017). We note that all simulations have a initial gas particle mass of 7100 $M_\odot$.

2. Simulations and Analysis Methods

In this study, we investigate the causes of starburst events using six zoom-in simulations from the FIRE-2 simulation suite. More specifically, we study what role flybys and mergers play in inducing starbursts. In this section, we describe the simulation sample, the halo identification and tracking method, the SFR and torque calculation, and the detrending of the SFR.

2.1. The Simulations

We analyze the FIRE-2 simulations from the Feedback in Realistic Environments (FIRE) project (P. F. Hopkins et al. 2014, 2018), a set of cosmological "zoom-in" simulations run with the GIZMO code (P. F. Hopkins 2015)[12] from redshift 99 to 0. The simulations use a Meshless Finite Mass hydrodynamic solver with explicitly modeled star formation and feedback processes. These processes include energy, momentum, mass, and metal fluxes arising from SNe types I&II, stellar mass-loss (O-star and AGB), radiation pressure (UV and IR), photoionization, and photoelectric heating. For more information about the simulations and feedback prescriptions, please refer to P. F. Hopkins et al. (2018).

In this paper, we study the effect of tidal interactions on the star formation activity around Milky Way-mass star-forming galaxies. To match with the mass of the Milky Way galaxy, we select the galaxies according to their dark matter halo mass at $z = 0$ in the zoom-in simulations from the FIRE-2 simulation suite (A. Wetzel et al. 2023). The selected galaxies and their characteristics are listed in Table 1. A subgrid model for turbulent metal diffusion is included for all simulations in our selected sample. The effects of magnetic fields or cosmic rays are not included in the selected runs.

[11] http://fire.northwestern.edu

[12] http://www.tapir.caltech.edu/~phopkins/Site/GIZMO.html

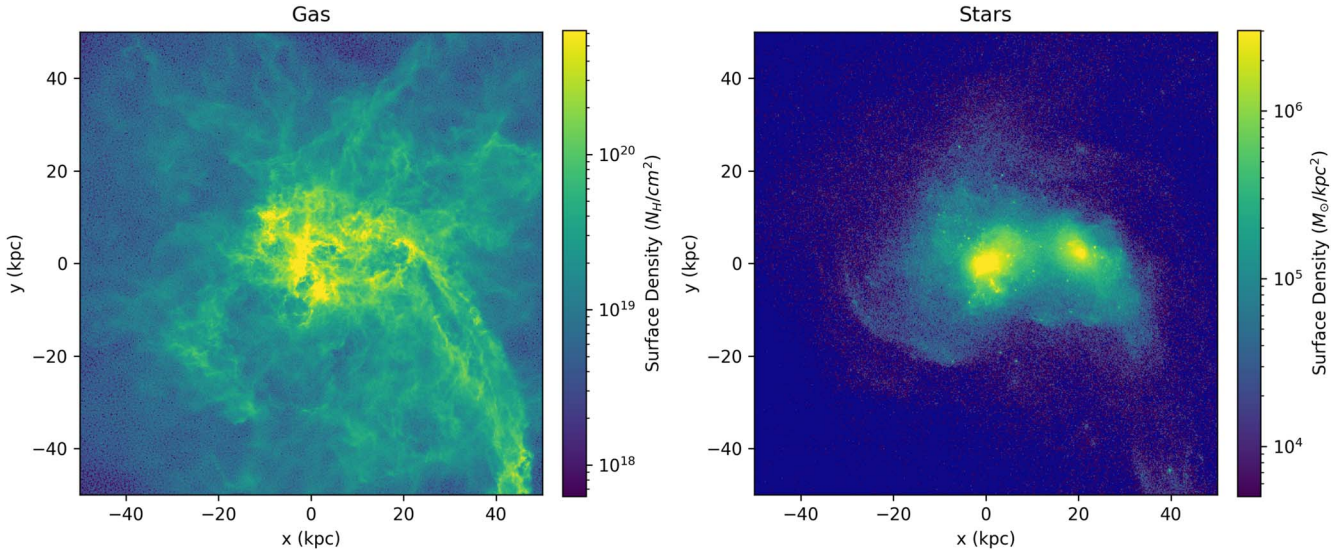

Figure 1. A major merger in the m12m simulation run at $z = 1.6$ with a stellar mass ratio of 0.66. The distance between the two galaxies is 22 kpc. The left-hand panel shows the gas distribution of the central and companion galaxies, and the right-hand panel shows the stellar component of the galaxies.

2.2. Identifying and Tracing Halos

To study the effect of galaxy interactions on the star formation activity of the main galaxy, we need to identify and trace the main halo and the companion halos across all simulation snapshots. Each galaxy simulation has 600 snapshots across cosmic time, leading to a snapshot time resolution of 20–25 Myr. We identify the (sub)halos using the Robust Overdensity Calculation Using K-Space Topologically Adaptive Refinement (ROCKSTAR) 6D phase-space temporal halo finder (P. S. Behroozi et al. 2013a). ROCKSTAR is based on adaptive hierarchical refinement of friends-of-friends groups in six phase-space dimensions and the time dimension. The halos are identified using dark matter particles, when the average density is 360 times the mean matter density within R_{360} with bound mass fraction >0.4, and when there are at least 30 dark matter particles in a halo. Merger trees are constructed using *consistent-tree* (P. S. Behroozi et al. 2013b) with the halo catalog generated by ROCKSTAR for each snapshot. We have compared the output of ROCKSTAR with other halo finders and found similar results, though ROCKSTAR tends to be more robust in tracing subhalos when they are close to the center of a larger halo. Further details of the ROCKSTAR halo catalogs are discussed in A. Wetzel et al. (2023).

Within each zoom-in simulation, the main halo is selected according to its mass at $z = 0$—the most massive halo in the high-resolution region is identified as the main halo. Among the main halo's progenitors at previous snapshots according to the results from *consistent-tree*, the one with the smoothest and generally monotonically increasing mass history is selected as the central halo through all snapshots from $z = 3.6$ to $z = 0$.

For the potential companion galaxy sample, we select the 1000 most massive halos at $z = 3.6$ in each simulation and trace them to $z = 0$, though we note that many fewer halos actually interact with the central galaxy. The large initial selection ensures that all progenitor halos that merge into a galaxy that interacts with the central halo are accounted for. We calculate the stellar mass of the companion galaxies by summing over all star particles within 10% of the virial radii as reported by ROCKSTAR.

Figure 1 shows an example of the distribution of the gaseous and stellar component of the main halo in the m12m simulation run at $z = 1.6$, where the central galaxy is undergoing a major merger. We present an example of the companion galaxy identification results in Figure 2: we plot the distance of all the nearby halos with dark matter mass above $10^9 M_\odot$ from the center of the main halo as a function of cosmic time for the m12m simulation run.

2.3. Identifying and Categorizing Halo Interactions

With the primary halo identified and traced across all simulation snapshots, we are able to filter our investigation to only halos that interact with the main galaxy for further analysis. These halos are identified by finding galaxies with a stellar mass greater than 1% of the simulations' primary galaxy that approach within 100 kpc of it. The population of satellites selected using this criterion is broadly similar to the satellites selected if total mass was used as the criteria. We note that tracing halos close (∼kpc) to the central galaxy is challenging given the confusion of particles in the snapshot, so we limit the tracing of these subhalos to 10 kpc from the center of the main halo.

The identified galaxies may either merge into the main galaxy after their final approach or simply flyby the main galaxy with minimal exchange of mass. For the purpose of this study, we deem both of these cases to be interactions. We do note, however, that all galaxies in these simulations with a stellar mass ratio of $\mu \geqslant 0.25$ that approach the main galaxy closer than 100 kpc do eventually merge within 1–2 Gyr.

We further subdivide the interactions into three mass ratio-related categories,[13] the major interactions, with stellar mass ratios of $\mu \geqslant 0.25$, the minor interactions, with $0.1 \leqslant \mu < 0.25$, and the mini-interactions, with $0.01 \leqslant \mu < 0.1$. We use these classifications to enable fine-grained analysis of the effect of the interactions.

[13] In this paper, we use the mass ratio calculated at each snapshot. There are other studies of galaxy simulations (e.g., T. J. Cox et al. 2008; G. Martin et al. 2017) that use the maximum mass of the secondary galaxy prior to coalescence for the calculation of the mass ratio for all snapshots in which the merging companions are involved in.

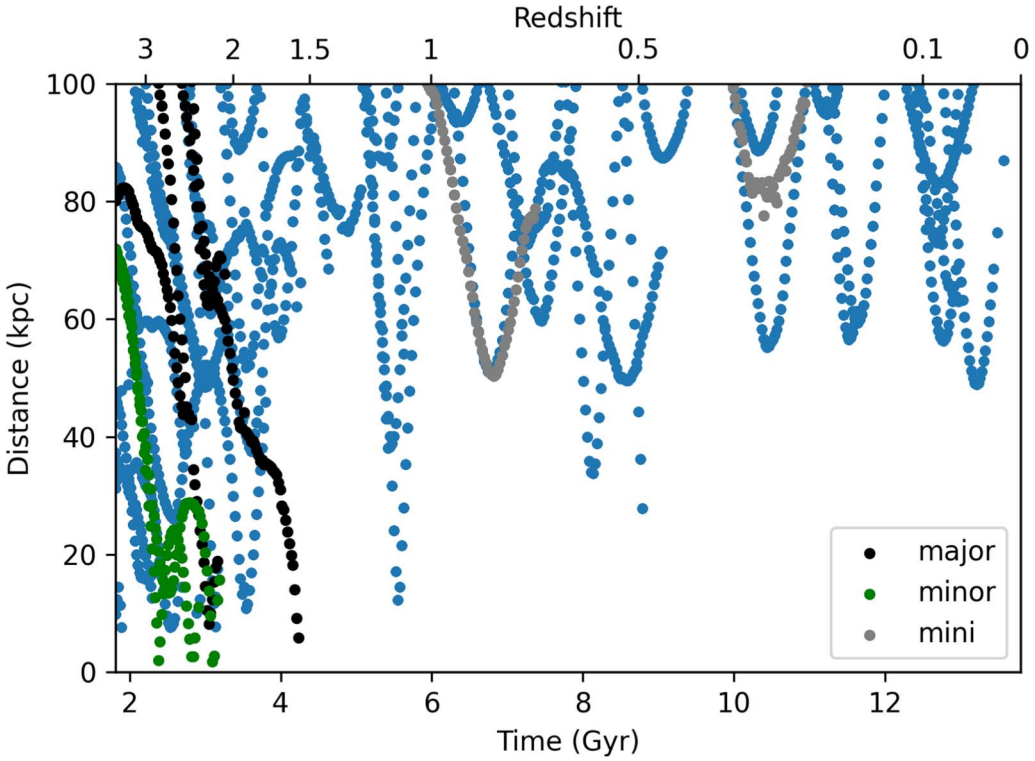

Figure 2. The distance of all the nearby halos with dark matter mass above $10^9 M_\odot$ to the center of the main halo as a function of cosmic time for the m12m simulation run. The black dots show the distance of galaxies in snapshots with major interactions, where the companion-to-central galaxy stellar mass ratio is above or equal to 0.25; the green and gray dots represent galaxies involved in minor interactions ($0.1 \leqslant \mu < 0.25$) and mini-interactions ($0.01 \leqslant \mu < 0.1$), respectively; while the blue dots show galaxies with stellar mass ratios smaller than 0.01 (but halos masses larger than $10^9\ M_\odot$). The $R_{\rm vir}$ is 107 kpc at $z = 3.6$, and 341 kpc at $z = 0$.

Each of the snapshots across all simulations are classified based on if the central galaxy is undergoing an interaction by the criteria above. We note that more than one galaxy could meet the criteria for a given snapshot, but the mass-ratio classification is based on the most massive of those galaxies. These classifications are further verified manually to remove any misclassifications due to confusion in companion halo parameter measurement: for instance, removing artificially inflated masses of close-passing satellites where simulation particles from the main galaxy are erroneously associated with the satellite. Across the six simulations, we identify that the main galaxy is undergoing some form of interaction ∼40% of the time.

It is worth noting that the zoom-in simulations used in this study were selected only to match the halo mass of the Milky Way at $z = 0$ and not specifically selected to match any other property of the Galaxy, including its relative quiescence at low redshift (A. Wetzel et al. 2023). Despite that, all major mergers in the sample typically occur at early times ($z > 1.2$), consistent with the Milky Way's decreasing merger rate at late times (e.g., C. J. Conselice et al. 2003; E. F. Bell et al. 2006; C. N. Lackner et al. 2014). Furthermore, we also note that the minimum distance of the satellite galaxy approaches increases at late times. We discuss these properties in more detail in Section 3.

2.4. Measuring Star Formation

To study the effect of the tidal interactions on the central galaxy, we need to know the exact times that starbursts occur in the galaxies. We calculate the short-term SFR of each snapshot by summing over the mass of stars formed within 5 Myr, corresponding to the age at which the massive stars producing ionizing radiation evolve off the main sequence, and divide the total mass of newly formed stars by the time interval (5 Myr). We do so for all stars within 10 kpc of the center of the galaxy, consistent with the size of the stellar disk.

As a check of the robustness of our calculated SFR, we have performed the same calculation with radii up to 50 kpc, and for stars formed within different time intervals (<20 Myr, the default time between snapshots), and found that the SFR history is generally not sensitive to the choice of the radius or the time interval.

The raw SFR has large-scale secular variations on several hundred million-to-billion year timescales. To determine the short time (∼10 Myr) effect of interactions, which happen on timescales of 10−100 Myr (e.g., W. C. Keel et al. 1985; J. E. Barnes & L. E. Hernquist 1991; P. F. Hopkins & L. Hernquist 2010; E. Cenci et al. 2024), we also utilize a detrended SFR. We detrend the SFR by calculating a smoothed SFR with a Gaussian filter with $\sigma = 25$ snapshots (∼550 Myr), and then divide the original raw SFR by the smoothed to provide a unitless over/under abundance of star formation as compared to the secular trend. This makes it possible to compare the results across different redshifts and between different galaxies.

2.5. Measuring Interaction Torques

It has been suggested that one possible mechanism for the enhancement of star formation from galaxy interactions is the torque exerted by the stars in the central galaxy on the gas in the same galaxy, as a result of the perturbation by the companion galaxy (J. C. Mihos & L. Hernquist 1994, 1996; J. E. Barnes & L. Hernquist 1996; P. F. Hopkins et al. 2013). The mutual torque between the stars and gas in the main galaxy leads to a decrease in the angular momentum of the gas, and

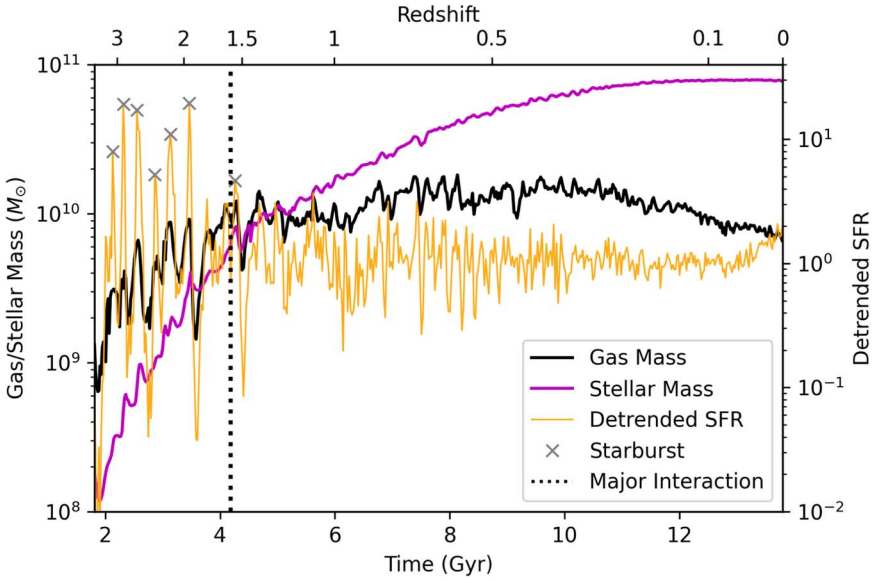

Figure 3. The gas mass (the black line), the stellar mass (the magenta line), and the detrended SFR (the orange line) of the central galaxy in m12m as a function of cosmic time. The black dotted vertical line marks the end of a major merger event, which is defined as when the center of the satellite galaxy is within 10 kpc of the central galaxy. The gray Xs mark starburst events, where the detrended SFR is greater than 4. There are seven such starburst events; during the same period, there is one major merger and three minor interactions, suggesting that most of the starbursts are not associated with major or minor interactions. All of the simulated galaxies in the sample have mass and star formation histories that are qualitatively similar with those shown here. Similar plots for other sample galaxies are shown in Figure 4, and in Figures 11 and 12 in Appendix C.

thus induces gas inflow to small radii, thereby enhancing the SFR.

The calculation of the torque between the stellar and gaseous components for all our snapshots for all our central galaxies is computationally prohibitively expensive. In this work, we used the torque from the companion galaxies on the gas particles in the central galaxy as a proxy; we assume this torque is proportional to or has a monotonic relationship with the torque from stars to the gas in the central galaxy.

To quantify the impact of interactions on the star formation activity in the main galaxy, we calculated the torque exerted on the gas particles in the central halo from the nearby halos. The galaxies within 1500 kpc of the main halo at each snapshot are included in the calculation. The expression of the torque is $\boldsymbol{r} \times \boldsymbol{F}$, where $\boldsymbol{r}$ is the vector from the center of the main galaxy to the gas particle in the disk, and $\boldsymbol{F}$ is the gravitational force vector,

$$\boldsymbol{F} = \frac{GM_{\rm f}m_{\rm i}}{R^3}\boldsymbol{R}, \tag{1}$$

where G is the gravitational constant, $M_{\rm f}$ is the dark matter mass of the flyby halo as reported by ROCKSTAR, $m_{\rm i}$ is the mass of the gas particle in the main galaxy, and $\boldsymbol{R}$ is the vector from the gas particle to the center of the flyby galaxy. We perform the calculation by summing over the torque from the companion halos on every gas particle in the main halo,

$$\boldsymbol{\tau} = \sum_{M_{\rm f}}\sum_{m_{\rm i}} \boldsymbol{r} \times \frac{GM_{\rm f}m_{\rm i}}{R^3}\boldsymbol{R}. \tag{2}$$

We calculated this torque in spherical shells of width $\Delta R = 1$ kpc from the center of the main galaxy to $R = 20$ kpc. At large radii, this procedure will include gas not in the galactic disk. We did this for each snapshot for all the galaxies we discuss. We also use specific torque in our analysis, the specific torque is calculated as the torque divided by the total gas mass in the region.

We note that the torque calculated at each snapshot through this procedure is the sum of the torque of all halos within 1.5 Mpc on the central galaxy. However, these torques are dominated by the effect of one or two halos for any given snapshot.

3. Results

The FIRE m12 series of galaxy simulations provide a consistent picture of the interaction and star formation history of Milky Way-mass galaxies. While the only selection criterion applied to these galaxies is that they must match the halo mass of the Milky Way at $z = 0$, they all appear to have similar behavior (Figures 3 and 4)—all major mergers occur at early times, between $1.2 < z < 3.6$. The merger rate of the galaxies decreases with redshift at late times (e.g., P. F. Hopkins et al. 2010; V. Rodriguez-Gomez et al. 2015; K. B. Mantha et al. 2018). The star formation in the galaxies goes from bursty to more stable at $z \sim 1$, which also coincides with the onset of disk formation, and the disks then become thinner over time, e.g., S. Yu et al. (2021, 2023), Z. Hafen et al. (2022), and F. McCluskey et al. (2024). For the mergers identified through these simulations, some are able to bring gas into the main halo (i.e., gas-rich mergers), while others do not (i.e., gas-poor mergers), but in neither of these cases do most mergers have a significant effect on the overall SFR of the galaxy, nor does it consistently lead to a burst in star formation at the time of the merger. For Milky Way-mass halos, it appears that the time, size, or gas-richness of the mergers have no significant impact on the overall star formation history or present day SFR of the galaxy. We also note that the durations of the starbursts (when the detrended SFR is greater than 4) are 25–50 Myr.

3.1. Do Galaxy Interactions Trigger Starbursts?

While we do not see a significant impact on the overall star formation history due to interactions, they may yet be responsible for catalyzing specific starburst episodes within

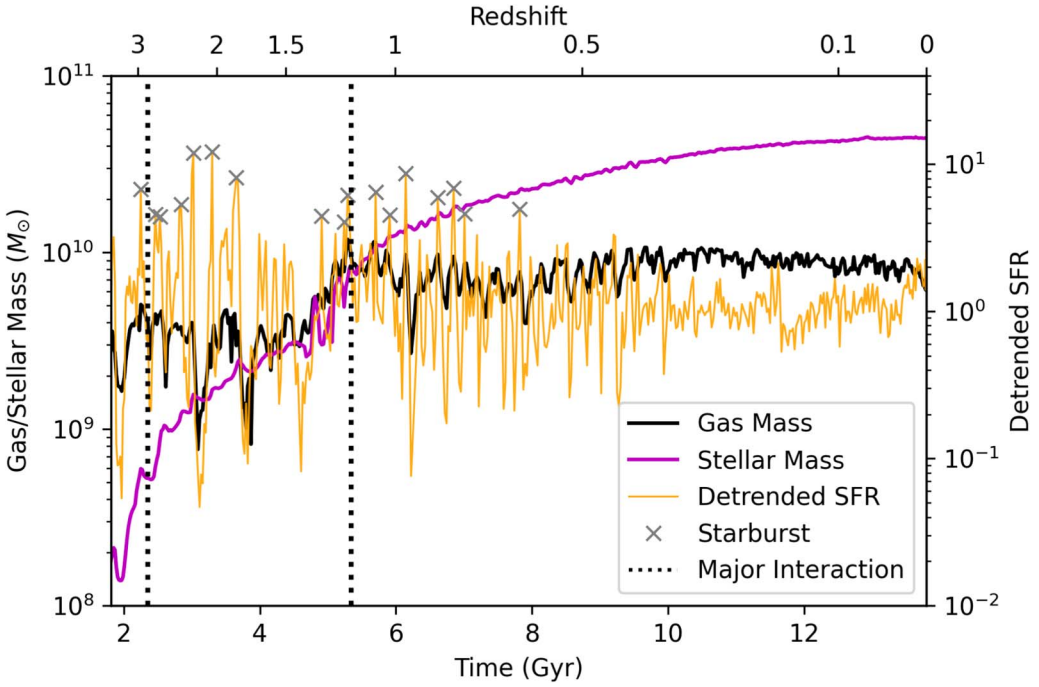

Figure 4. Similar to Figure 3, but for the simulated galaxy m12c. This is the only galaxy in the sample with a measurable increase of the gas mass due to a major merger. We note that the detrended star formation history appears similar to all other galaxies within our sample. We see 17 starbursts over the redshift range of the figure, while there are two major mergers and two minor interactions, suggesting that many of the starbursts are not caused by significant interactions.

the host galaxy. Specifically, the torque on the system due to the companion galaxy may produce a local starburst (or otherwise elevated SFR) at the time of closest approach. We approach this proposed starburst mechanism by asking the following question: does the SFR of a galaxy increase with the torque exerted on it from a companion galaxy?

To address this question, we measure the correlation between the detrended SFR of the main halo in each of these simulations and the torque exerted on the halo by any companion galaxy. We adopt a detrended SFR to minimize any statistical contamination from secular trends in the star formation history of the galaxy, as described in Section 2.4. We adopt the Spearman rank correlation coefficient as our metric of correlation, which provides a measure of the strength of correlation of two variables based on their rank within the sample. The calculated p-value from the Spearman correlation coefficient indicates the probability of the null hypothesis, i.e., the measured correlation occurring by chance. The Spearman correlation test has the benefit of being independent of the scaling of the two variables, being only a function of the rank order of the measurement within the samples. This is in contrast to other statistical correlation tests, such as the Pearson correlation test, which measures the linear correlation between the two variables. We have repeated our analysis with a Pearson correlation coefficient and find no significant differences in the overall results. We note that these correlation tests are designed to measure monotonic relationships, so more complex relationships between the variables would not be uncovered through this study.

In the left-hand panel of Figure 5, we present the sum of the torque exerted by the 50 nearby halos that exert the greatest gravitational force on the central galaxy for each simulation snapshot between $0 < z < 3.6$ for m12m. We note that although we calculate the torque for the top 50 halos, it is dominated by one or two halos for any given snapshot, due to the R^{-2} relationship between the companion galaxy distance and the torque. We also show the true and smoothed SFR on the same axis for comparison. Similar figures are available for all remaining simulations in Appendix A.

Visually, the number of spikes in the torque exerted by companion galaxies is fewer than the spikes in SFR, immediately indicating that the interaction with companion galaxies cannot be solely responsible for the starbursts within a central galaxy. In the literature, starbursts are often defined as having 2–4 times the SFR above the galaxy main sequence (e.g., G. Rodighiero et al. 2011; C. Schreiber et al. 2015; S. L. Ellison et al. 2020), $\mathrm{SFR_{starburst}} > 4 \times \mathrm{SFR_{GMS}}$. Another selection criterion used is the birthrate parameter (R. C. Kennicutt 1983), $b = \mathrm{SFR}/\langle \mathrm{SFR} \rangle$, i.e., the ratio between the current SFR and the mean SFR over the lifetime of the galaxy, and a galaxy is a starburst galaxy when $b \geqslant 3$ (N. Bergvall et al. 2016). In Figures 3 and 4, and Figures 11 and 12 in Appendix C, we mark the peaks in detrended SFR when the SFR is four times, or more, than the smoothed SFR. There are on average 11 starburst events per galaxy from $z = 3.6$ to $z = 0$ in our sample. On average, there are one major interaction and three minor interactions for each galaxy; the number of major/minor interactions and starburst events for each galaxy is shown in Table 2. Significant interactions cannot account for all or even most of the starbursts in the star formation history of the FIRE galaxies we examine.

We present the Spearman correlation coefficients (and related p-values) for the relationship between torque and detrended star formation for m12m in the right-hand panel of Figure 5. We note that the results of this correlation test are similar if we use the true SFR rather than the detrended, or if we use a Pearson correlation test rather than a Spearman test. Within the m12m simulation, we find there is no significant correlation between torque and SFR for snapshots, other than for major mergers, where a moderate but significant correlation

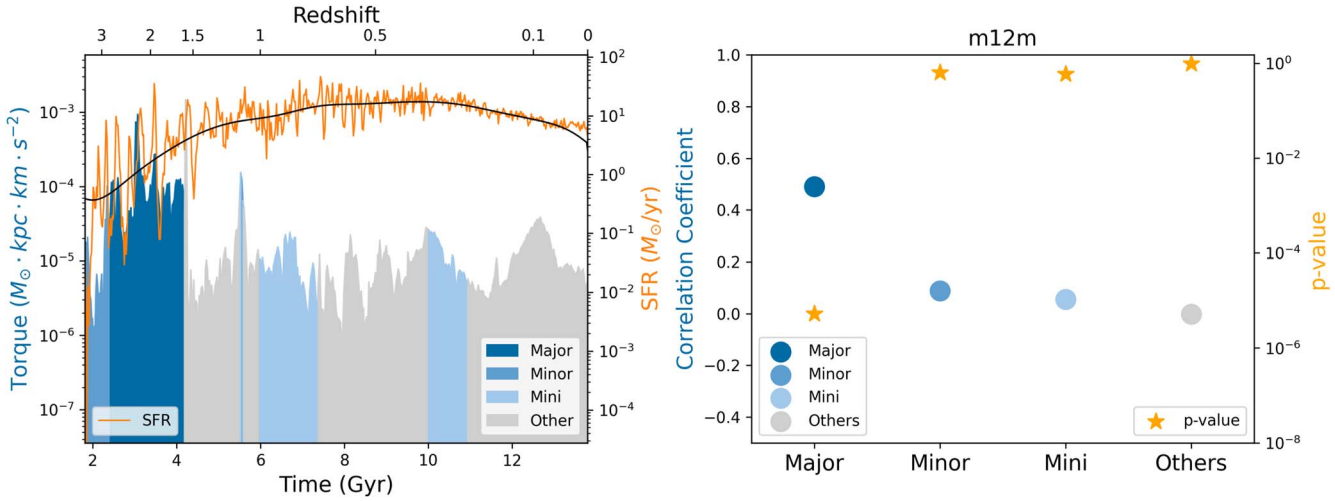

Figure 5. Left-hand panel: The torque and SFR for the simulated galaxy m12m. The torque is shown as shaded regions, assigned colors based on if they are undergoing an interaction during that snapshot. Dark blue indicates snapshots with major interactions ($\mu \geqslant 0.25$), medium blue with minor interactions ($0.1 \leqslant \mu < 0.25$), and light blue with mini-interactions ($0.01 \leqslant \mu < 0.1$). Light gray regions indicate no interaction. The SFR is plotted with the orange line, and the calculated smoothed SFR is plotted in black. Right: The Spearman correlation coefficient between the torque and the detrended SFR for snapshots within major interactions, minor interactions, mini-interactions, and other snapshots, shown as the blue and gray dots; the orange stars represent their corresponding p-values.

Table 2
The Number of Major Interactions, Minor Interactions, and Starbursts in Each Simulation; the Last Two Columns Show the Fraction of Time when the Galaxies are in Starburst Mode

Simulation	$M_\star^0$ ($M_\odot$)	Major Interactions	Minor Interactions	Starbursts	Starburst Fraction		Last Major Interaction Redshift
					($0.4 < z < 3.6$)	($0 < z < 3.6$)	
m12w	5.7×10^{10}	0	6	7	2.6%	1.6%	⋯
m12i	6.3×10^{10}	2	3	11	4.8%	3.0%	2.0
m12c	5.8×10^{10}	2	2	17	7.4%	4.7%	1.2
m12b	8.5×10^{10}	1	3	13	5.8%	3.7%	2.4
m12m	1.1×10^{11}	1	3	7	5.8%	3.7%	1.6
m12f	7.9×10^{10}	0	0	9	3.2%	2.0%	⋯

Note. Significant interactions cannot account for all or even most of the starbursts. There is no starburst after $z = 0.4$, and on average galaxies are in starburst mode for 3.1% of the time in $0 < z < 3.6$.

Table 3
Spearman Correlation Coefficients between the Torque and the Detrended SFR for Snapshots Involving Major Interactions, Minor Interactions, and Mini-interactions for the Six Simulations, with the p-values for the Correlation Coefficients Shown in the Parentheses

Simulation	Major Merger 1	Major Merger 2	Minor Interactions	Mini-interactions	Others
m12w	NA	NA	–0.21 (4×10^{-3})	0.26 (2×10^{-3})	0.15 (4×10^{-2})
m12i	0.76 (2×10^{-7})	0.85 (10^{-6})	0.12 (0.46)	0.27 (3×10^{-3})	–0.12 (5×10^{-2})
m12c	0.55 (3×10^{-3})	-7×10^{-2} (0.58)	0.00 (1.00)	0.11 (0.39)	1×10^{-1} (8×10^{-2})
m12b	9×10^{-2} (0.57)	NA	–0.14 (0.19)	0.22 (0.31)	-9×10^{-2} (0.10)
m12m	0.50 (3×10^{-6})	NA	0.12 (0.52)	9×10^{-2} (0.36)	5×10^{-2} (0.36)
m12f	NA	NA	NA	0.19 (6×10^{-3})	-5×10^{-2} (0.38)

does exist. This is similar for other galaxies, where there is a correlation of the SFR with four out of six major mergers. There are no major interactions in m12w and no major or minor interactions in m12f over the time interval we examined. Over the same time, the number of starbursts in m12w is five, and in m12f is nine. The same plot for the other simulated galaxies is shown in Figures 8 and 9 in Appendix A.

The correlation coefficients and their p-values for each type of interaction and each simulation are shown in Table 3. For major interactions, the detrended SFR has high correlation coefficients ($\geqslant$0.5) for four of the six simulated galaxies; for minor and mini-interactions, there is a statistically significant correlation coefficient for four of the 12 cases, and the correlation coefficient is around 0.2 for those cases; and for other snapshots, there is no information on the correlation between the SFR and the torque because the p-values are all high. This indicates that in some cases major interactions are correlated with starbursts but starbursts are more frequent than major interactions and occur even in the absence of major or minor interactions.

Table 4
Spearman Correlation Coefficients between the Torque and the Detrended SFR for Stacked Snapshots Involving Major Interactions, Minor Interactions, Mini-interactions, and Other Snapshots for the Six Simulations, with the *p*-values for the Correlation Coefficients Shown in the Third Column

Interaction Type	Correlation Coefficient	*p*-value
Major Interactions	0.41	2.0×10^{-12}
Minor Interactions	0.11	0.04
Mini-interactions	0.10	0.01
Others	0.05	0.05

Note. The torque and the detrended SFR are normalized in logarithmic space according to the maximum and minimum values within each interaction group in each simulation run.

The snapshots across the different simulations can be stacked by having the torque and detrended SFR values normalized in logarithmic space using the maximum and minimum values within each interaction type in each simulation. We can then perform the analysis using all snapshots with the different types of interaction in all simulations. Table 4 shows the correlation coefficient from the stacked snapshots. For major interactions, there is a positive and statistically significant correlation between the torque and the detrended SFR for major interactions, with a Spearman correlation coefficient of 0.41 and a *p*-value of 2.0×10^{-12}; for minor interactions, mini-interactions, and other snapshots, the *p*-values for the correlation coefficients are large, and therefore the correlation coefficients are not statistically significant.

Figure 6 shows the torques and SFRs of all the major interactions in all the simulations we analyzed. Three of the major interactions have a high correlation (>0.5) between torque and detrended SFR; while other major interactions show a low or no correlation between the two quantities. In comparison, the correlation between the gas mass increase rate and the detrended SFR is around 0.1 for all simulations. Consistent with our earlier finding, it appears that major interactions cause the starbursts in some cases but are not responsible for all or even most of the starbursts. This is expected because each burst will cause subsequent gas infall and potentially more bursts (A. L. Muratov et al. 2015; D. Anglés-Alcázar et al. 2017).

In Figure 7, we present the distributions of the detrended SFR from snapshots during major interactions, using snapshots up to 0.5 Gyr before and after the interaction as a control sample. We note that for the control sample, snapshots within the 0.5 Gyr time window where another major interaction is occurring have been excluded. If there was an enhancement in the SFR during major interactions, we would expect to see the distribution of the detrended SFR to be shifted for the major interaction sample. We find no significant difference between the two samples using a K-S test (*p*-value of 0.14), indicating that we find no measurable enhancement of the star formation during major interactions. We note that this analysis is insensitive to the distance criteria used for when an interaction begins (i.e., 100 kpc as discussed in Section 2.3), with the distributions being similar when the distance criteria is limited to 50 kpc.

We have shown that in our simulations, galaxy interactions do not cause the majority of starbursts, so starbursts can occur in the absence of a major merger. However, we also see instances of major mergers that do result in starbursts. To see why this might be the case, we also looked at the influence of orbital parameters of companion galaxies. For example, prograde mergers are more likely to excite resonant (E. D'Onghia et al. 2010) interactions between the gas and stars in the host and the orbital frequency of the perturber, so perhaps prograde mergers more often produce starbursts (E. D'Onghia et al. 2010). However, most of the companion galaxies in the major interaction sample are not in strictly prograde or retrograde orbits because the central galaxies have not developed well-formed disks yet. The inclinations between the angular momentum vectors of the orbits of the companion galaxies and the angular momentum vectors of the central galaxies are shown in Figure 10 in Appendix B for all simulations that involve major mergers. Thus, we do not have any evidence that the orbital parameters have a significant effect on the star formation in the host galaxy.

The detrended SFRs for m12m as shown in Figure 3 and similar figures for other runs (Figure 4, and Figures 11 and 12 in Appendix C) demonstrate that the SFR history across the simulations look similar regardless of the presence of major interaction events, transitioning from bursty to steady star-forming state during the redshift range in the analysis.

As shown in Figure 5, and Figures 8 and 9 in Appendix A, the star formation history of the galaxies across cosmic time are not dramatically affected by major interactions. Even in the cases where major interactions are present and the torques are strongly correlated with the starbursts, the major interactions do not leave a significant imprint on the total star formation history of the galaxies. The only exception is m12c, which has an abrupt jump in stellar mass right before the end of the second major merger, as shown in Figure 4 and Figure 8 in Appendix A.

4. Discussion

The above analysis of the m12 simulations indicates that the occurrence of starbursts in Milky Way-mass galaxies are mostly independent of interactions of companion halos. Furthermore, if any mechanism from a flyby or merger enhances the star formation within the central galaxy, its overall effect is weak.

A difficulty in the methodology of this analysis comes from the need for the central galaxy and companion galaxy to be separable and independently traceable. However, as the secondary galaxy approaches within 10 kpc of the center of the main halo, the simulation particles are substantially mixed, preventing a clean separation between the two components, as would be expected during the merger process. Consequently, any starburst immediately after the merger of the systems would be missed by the correlation metrics used. However, other studies have found that the majority of the star formation enhancement occurs prior to coalescence of the two systems (e.g., G. Martin et al. 2017), which we find to be consistent with this work as none of the systems show a starburst immediately after the completion of the merger.

The analysis conducted in this study is motivated by the suggestion of a specific proposed physical mechanism of interaction-induced star formation enhancement, i.e., torque-induced nuclear inflow of gas. While the overall analysis aims to identify any correlation between the companion galaxy behavior and star formation in the central galaxy, the detailed correlation analysis between the torque induced by the secondary galaxy and the SFR of the main galaxy is designed to specifically identify any effect of this pathway on starbursts. Other mechanisms of central-companion galaxy interplay have been suggested as possible sources of star formation enhancement, including shocks and tidal compression (C. J. Jog & P. M. Solomon 1992; F. Renaud et al. 2014, 2019); however, a

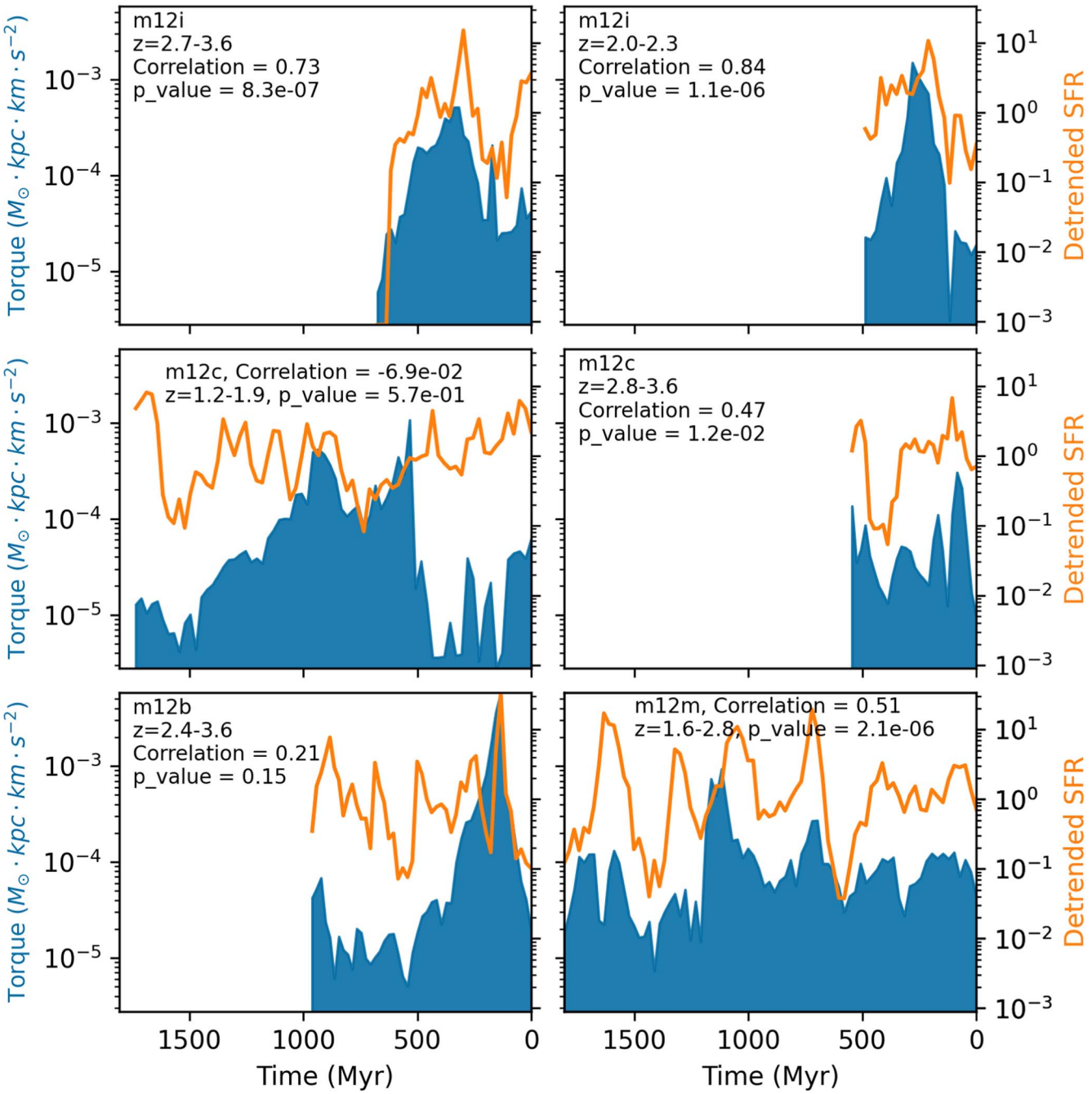

Figure 6. The torque and the detrended SFR during major interaction snapshots in the six simulation runs. The x-axis shows the time until the final merger. In the analysis a merger starts when a halo with stellar mass ratio $\mu \geqslant 0.25$ is within 100 kpc of the center of the central galaxy, and ends when the companion galaxy is within 10 kpc of the center of the central galaxy and does not reappear outside that radius as a separate halo again. Each major merger is shown as a single panel, some panels involve multiple major mergers occurring close in time. There are six major mergers in all the simulated galaxies. The simulated galaxies m12f and m12w do not have any major interaction between $z = 3.6$ and $z = 0$.

specific analysis of these pathways is beyond the scope of this current work. However, we note that the analysis conducted in this work puts an upper envelope on the total star formation enhancement that could be produced by any form of interaction for Milky Way-mass galaxies independent of physical mechanism.

4.1. Comparison to Observations

The major mergers in this study occur during the redshift range $z = 1.2-3.6$, which we can compare to observational studies of galaxies in that same time range.

W. J. Pearson et al. (2019) and A. Silva et al. (2018) both compare the star formation activity of merging and nonmerging galaxies through the HST CANDELS survey: in both cases, they find an insignificant difference between the merger and nonmerger SFRs between galaxies up to a redshift of 4. In Figure 7, we show the histogram of the SFRs of each snapshot broken into major merger and nonmajor merger populations, showing no statistical difference between the populations, in excellent agreement with these observational works.

A wider observational study by S. L. Ellison et al. (2008) using SDSS galaxies finds an enhancement in the star formation of galaxies with close (<40 kpc) interactions as

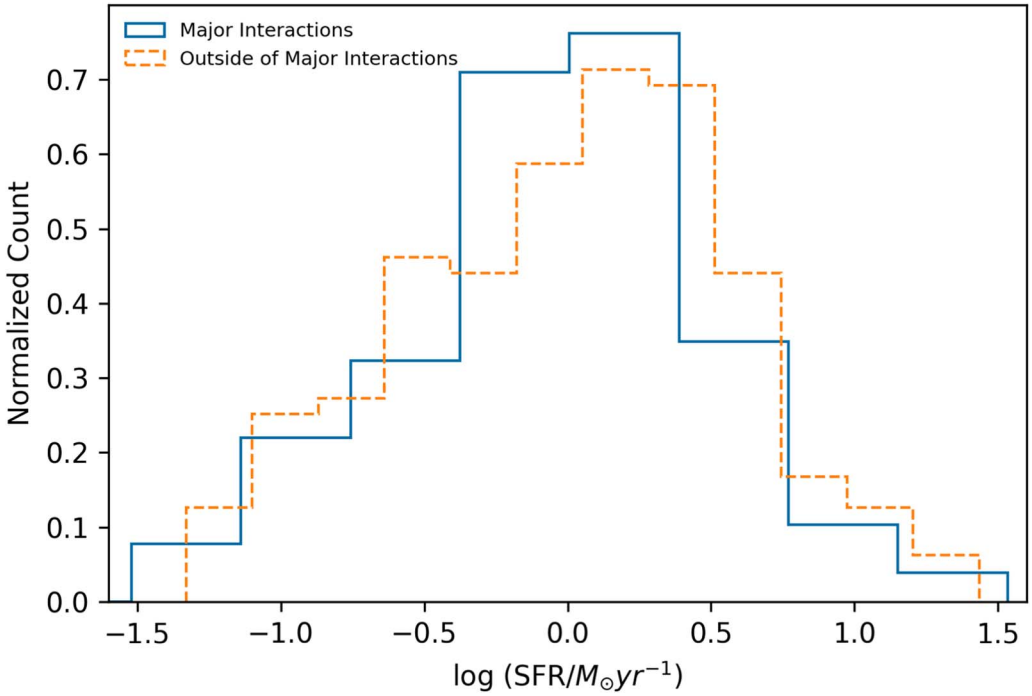

Figure 7. The normalized histogram of the detrended SFR for snapshots during a major interaction (blue solid line), and 0.5 Gyr before and after the interactions (orange dashed line). The two distributions show no significant difference, indicating that there is no statistical enhancement of the SFR at the time of major interactions as compared to outside of these major interactions.

compared to field galaxies, though the effect is most prominent at the closest radii and with mass ratios greater than 0.5. We note that the statistical elevation measured by S. L. Ellison et al. (2008), up to a 70% increase in the average SFR, would not constitute a "starburst" event for the purposes of this study. This result is overall consistent with the mild correlation we measure between the torque and the SFR for major interactions.

Furthermore, the starburst rates inferred from these simulations are largely consistent with observational studies. We infer a starburst rate of 3% between $0 < z < 3.6$, with no starburst occurring after $z = 0.4$ (Table 2). About 15% of the starbursts occur within 0.5 Gyr after major interactions, consistent with the results from A. L. Muratov et al. (2015) and D. Anglés-Alcázar et al. (2017), which suggest bursts followed by gas recollapsing onto the central halo to cause subsequent bursts.

N. Bergvall et al. (2016) find a starburst rate of 1% for $10^9 M_\odot < M_{\rm gas+stars} < 10^{11.5} M_\odot$ galaxies in the local universe, albeit with a different definition of starburst corresponding to events raising the star formation to three times the lifetime average SFR of the galaxy, versus our threshold of four times the local average SFR. G. Rodighiero et al. (2011) find a starburst rate of 2%−3% for $10^{10} M_\odot < M_* < 10^{12} M_\odot$ galaxies at $1.5 < z < 2.5$ using a starburst threshold of four times the typical SFR as inferred from the galaxy main sequence. Overall, the FIRE simulations are consistent with the observed statistics of starburst events from observations.

4.2. Comparison with Previous Simulations

The FIRE simulations provide a high-resolution cosmological view of the evolution of Milky Way-mass galaxies, taking into account their full assembly and environmental history. This provides us with a unique comparison to other simulations that focus on isolated systems and other cosmological simulations. We do note that the burstiness of the star formation in the FIRE simulations is due to their high-resolution of galaxy ISM, which have no real analog in other simulation work discussed here (A. Wetzel et al. 2023).

This work is consistent with the analyses from other cosmological simulations, such as G. Martin et al. (2017), using the Horizon-AGN simulations. They also find that the merger contribution to stellar mass growth is small at all redshifts, and is not a dominant driver across the life of the galaxy; see also D. Kereš et al. (2005) for the same conclusion.

Furthermore, the current analysis provides useful context to simulations of merging galaxies in isolated volumes: V. Perret et al. (2014) modeled major and minor interactions, using idealized galaxies with high gas fractions at $1 < z < 2$, finding no enhancement of overall star formation. Additionally, idealized simulations provide opportunities to tweak experimental parameters to measure their effect. For instance, J. Fensch et al. (2017) infer the efficiency of high-redshift mergers to be significantly lower than those at low-redshift, while J. M. Scudder et al. (2015) find that galaxies with high gas fractions have higher baseline SFRs and weaker star formation enhancements than lower gas fraction galaxies; B. Robertson et al. (2006) find a similar relationship between SFRs during the first pericentric passage and final coalescence. J. Moreno et al. (2021) use high-resolution, isolated simulation volumes of major mergers to identify a global ∼35% enhancement of the SFR in the primary galaxy due to a merger.

However, with the cosmological perspective provided by the FIRE simulations, we find that low-redshift interactions with Milky Way-mass galaxies are rare in comparison to higher redshifts, and the star formation history and gas fractions of these galaxies have little variation for samples at the same redshift. Consequently, the cosmological perspective allows us to exclude physical mechanisms that are unlikely to proceed due to the environmental and merger history of such halos.

One finding from E. Cenci et al. (2024), which also used cosmological zoom-in simulations with FIRE-2 physics, is that major mergers result in the largest difference in the proportion of interacting starburst and interacting nonstarburst galaxies. This is consistent with the mild correlation in minor and mini-interactions between torque and detrended SFR in this paper.

5. Conclusions

We use six cosmological zoom simulations of Milky Way-mass star-forming galaxies from the FIRE-2 simulation suite to investigate whether interactions with flyby or merging halos may induce starbursts in such galaxies. We trace interacting halos around the central galaxy for each simulation suite and measure the torque of these halos on the central galaxy's gas content. We measure the correlation between the torque and star formation during all merger and flyby events from $z = 3.6$ to $z = 0$, separating the interactions into major, minor, and mini-interactions based on the stellar mass ratio of the galaxy pairs. We similarly measure the baseline torque-star formation correlation using all other snapshots. Our main conclusions are as follows:

(i) For major interactions, there is a positive and statistically significant correlation between the torque from nearby galaxies on the gas of the central galaxy and the detrended SFR. The correlation results in a Spearman coefficient of 0.41 with a p-value of 4.1×10^{-12} (Table 4).

(ii) There is no one particular pathway where interactions lead to starbursts in the central galaxy—some major interactions cause starbursts, but most starbursts are not caused by galaxy interactions.

(iii) For minor interactions, mini-interactions, and all other snapshots in the sample, there is no statistically significant correlation between torque and star formation (Table 4).

(iv) The transition from bursty to steady star formation state appears to be independent of the interaction history of the galaxies.

(v) Most halo interactions do not leave a significant imprint on the overall trend of the star formation history of Milky Way-mass galaxies.

This work argues for a paradigm where the star formation processes of Milky Way-mass galaxies is not strongly dependent on the physics of interactions (flybys or mergers) but rather due to cosmological environments that control the overall accretion rates of the halos. In this picture, Milky Way-mass galaxies undergo most of their major interaction activities at early times, undergo only a handful of major mergers at most, and have star formation histories, in particular, burstiness, driven primarily by internal dynamics.

Acknowledgments

N.W.M. acknowledges the support of the Natural Sciences and Engineering Research Council of Canada (NSERC; RGPIN-2023-04901). This work was performed in part at the Aspen Center for Physics, which is supported by National Science Foundation grant PHY-2210452. D.K. was supported by NSF grant AST-2108324. A.W. received support from NSF, via CAREER award AST-2045928 and grant AST-2107772, and HST grant GO-16273 from STScI. C.A.F.G. was supported by NSF through grants AST-2108230 and AST-2307327, by NASA through grant 21-ATP21-0036, and by STScI through grant JWST-AR-03252.001-A. Support for P.F. H. was provided by NSF Research Grants 1911233, 20009234, 2108318, NSF CAREER grant 1455342, NASA grants 80NSSC18K0562, HST-AR-15800. The simulations presented here used computational resources granted by the Extreme Science and Engineering Discovery Environment (XSEDE), which is supported by National Science Foundation grant No. OCI-1053575, specifically allocation TG-AST120025 and resources provided by PRAC NSF.1713353 supported by the NSF; Frontera allocations AST21010 and AST20016, supported by the NSF and TACC; Blue Waters, supported by the NSF; and Pleiades, via the NASA HEC program through the NAS Division at Ames Research Center. The analysis of the FIRE simulation data was run on the CITA computing cluster "Sunnyvale." Computations were performed on the Niagara supercomputer (M. Ponce et al. 2019) at the SciNet HPC Consortium (C. Loken et al. 2010). SciNet is funded by Innovation, Science and Economic Development Canada; the Digital Research Alliance of Canada; the Ontario Research Fund: Research Excellence; and the University of Toronto. The data used in this work were, in part, hosted on facilities supported by the Scientific Computing Core at the Flatiron Institute, a division of the Simons Foundation.

The research made use of the following software: SCIPY,[14] NUMPY[15] (S. van der Walt et al. 2011), MATPLOTLIB[16] (J. D. Hunter 2007), and YT[17] (M. J. Turk et al. 2011).

Data Availability

A public version of the GIZMO code is available at http://www.tapir.caltech.edu/~phopkins/Site/GIZMO.html. FIRE-2 simulations are publicly available (A. Wetzel et al. 2023) at http://flathub.flatironinstitute.org/fire. Additional data, including initial conditions and derived data products, are available at https://fire.northwestern.edu/data/.

Appendix A
Torque and Detrended SFR Figures

Figure 5 in the main text shows the torque and the SFR along with the correlation coefficients and associated p-values for different interaction groups for the simulated galaxy m12m. Figures 8 and 9 in this appendix show the same relationship for the other simulated galaxies in this study. The values of the correlation coefficients are shown in Table 3.

[14] http://scipy.org
[15] http://numpy.org
[16] http://matplotlib.org
[17] http://yt-project.org

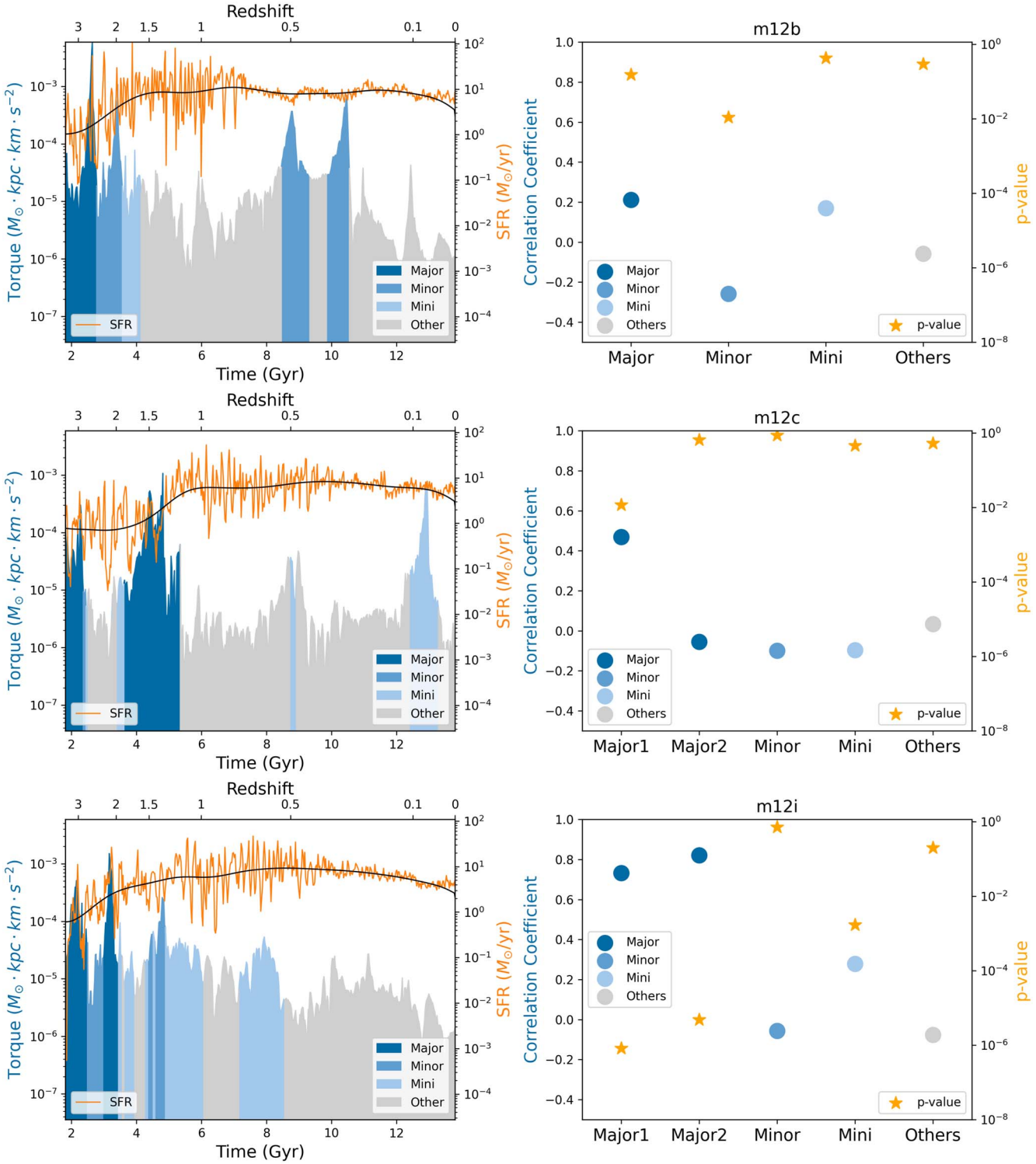

Figure 8. Analogous to Figure 5, but for the simulated galaxies m12b, m12c, and m12i.

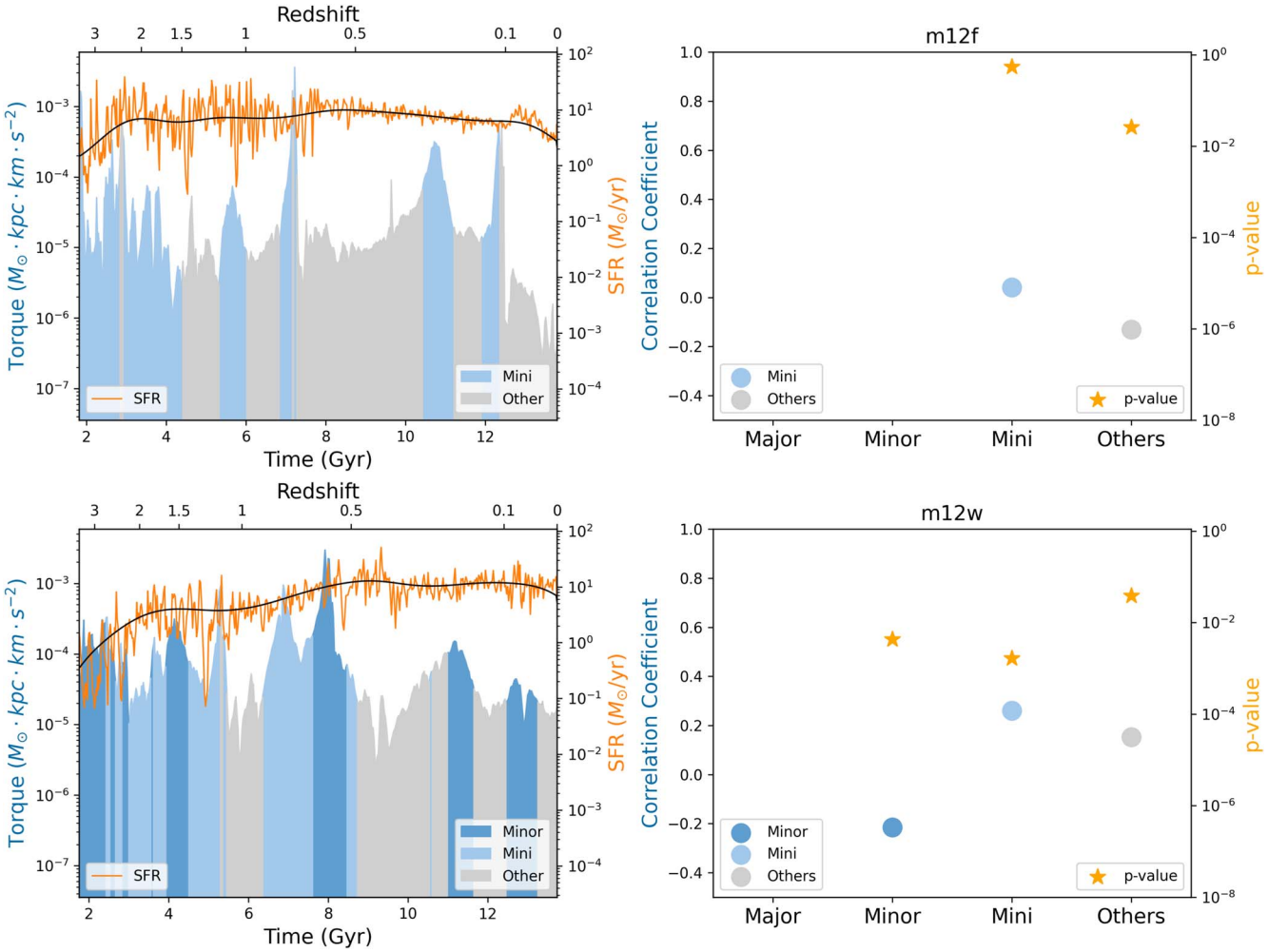

Figure 9. Analogous to Figure 5, but for the simulated galaxies m12f and m12w.

Appendix B
Inclination Figures

To study the impact of retrograde and prograde orbits on the correlation between the torque and the SFR, we calculated the angle between the angular momentum vector of the main galaxy and the angular momentum vector of the companion galaxy for major interactions as a function of cosmic time for all snapshots undergoing major interactions, shown in Figure 10.

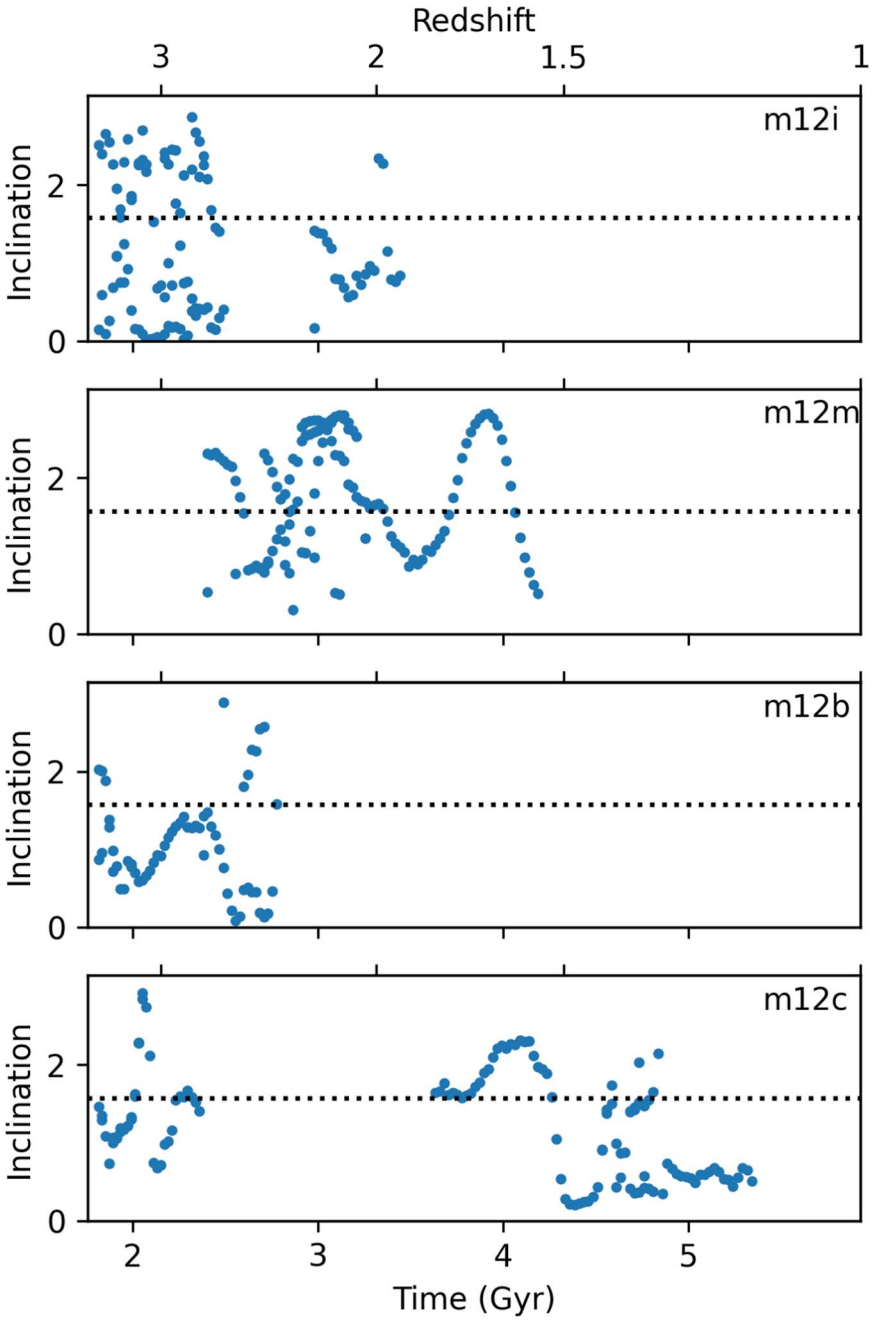

Figure 10. The angle (in radians) between the angular momentum vector of the main galaxies and the angular momentum vector of the companion galaxies for major interactions as a function of cosmic time for the simulation runs with major interactions.

Appendix C
Gas Mass, Stellar Mass, and Detrended SFR Figures

This section contains Figures 11 and 12 of gas mass, stellar mass, and the detrended SFR as a function of cosmic time; the plots for m12m (Figure 3) and m12c (Figure 4) are included in the main text, and the same plots for the other simulated central galaxies are shown in this section. All of the simulated galaxies in the sample have mass and star formation histories that are qualitatively similar.

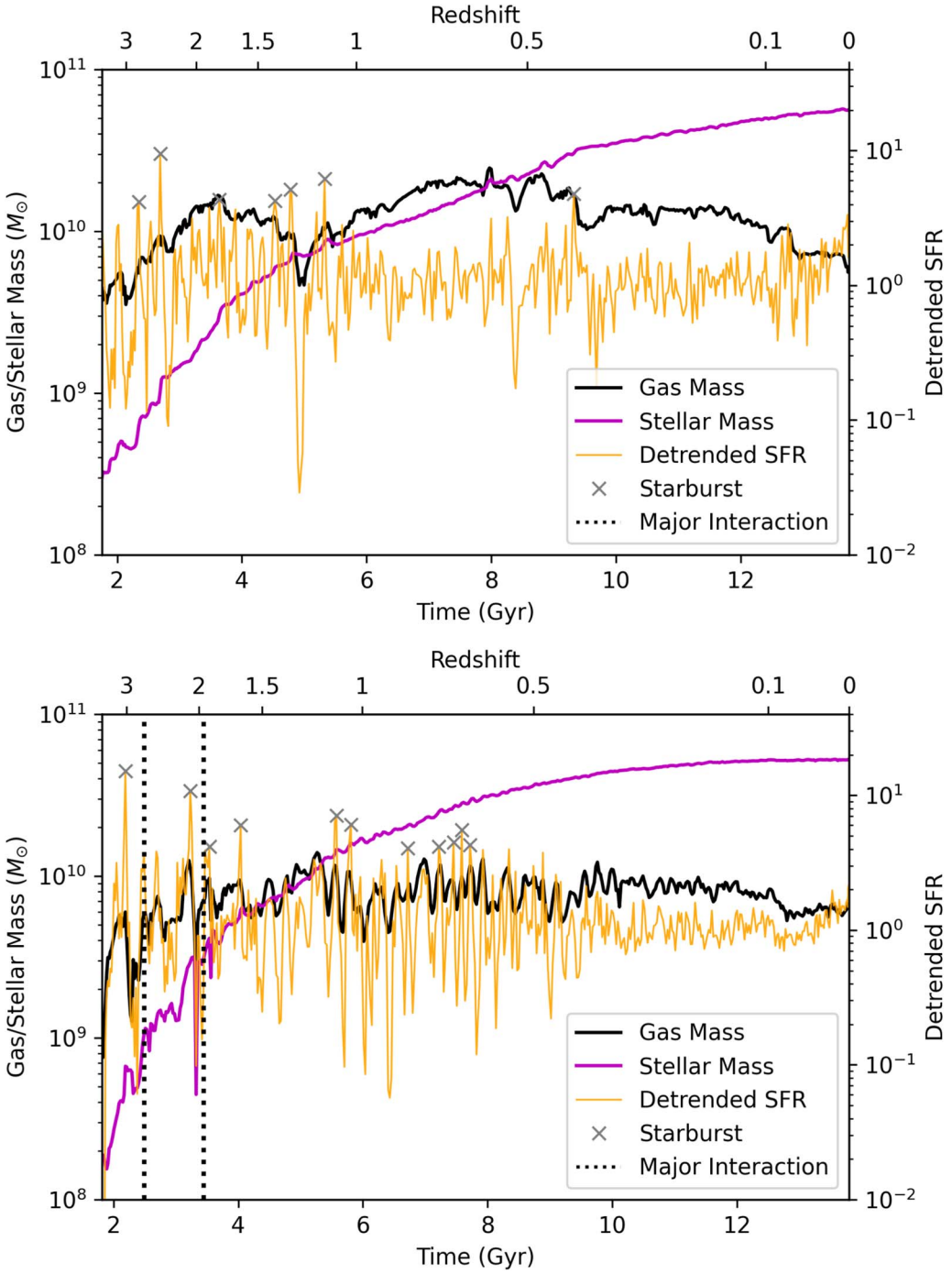

Figure 11. Analogous to Figure 3, but for the simulated galaxy m12w and m12i.

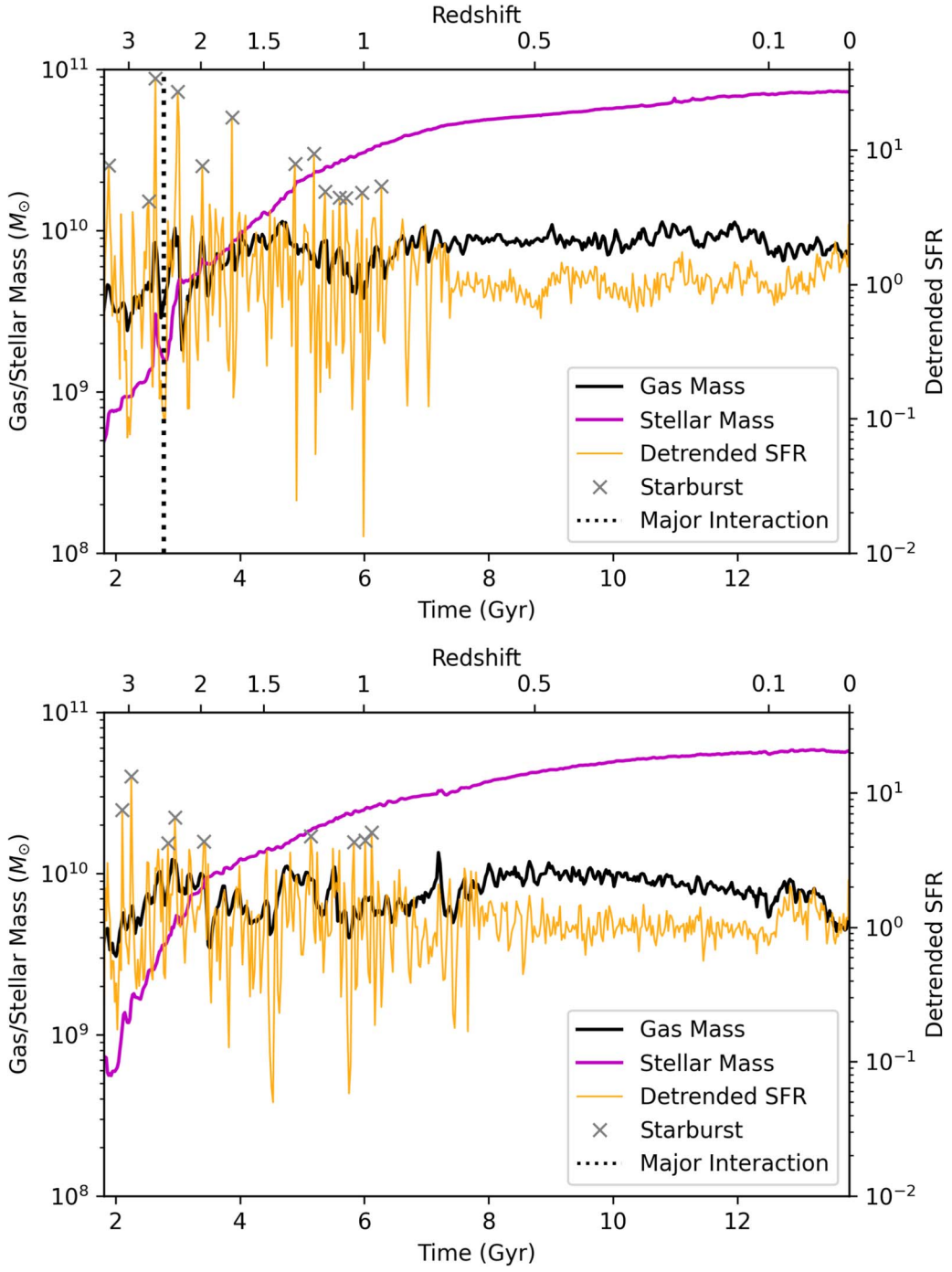

Figure 12. Analogous to Figure 3, but for the simulated galaxy m12b and m12f.

ORCID iDs

Fei Li (李菲) https://orcid.org/0009-0009-0483-5762
Mubdi Rahman https://orcid.org/0000-0003-1842-6096
Norman Murray https://orcid.org/0000-0002-8659-3729
Dušan Kereš https://orcid.org/0000-0002-1666-7067
Andrew Wetzel https://orcid.org/0000-0003-0603-8942
Claude-André Faucher-Giguère https://orcid.org/0000-0002-4900-6628
Philip F. Hopkins https://orcid.org/0000-0003-3729-1684
Jorge Moreno https://orcid.org/0000-0002-3430-3232

References

Alonso, M. S., Tissera, P. B., Coldwell, G., & Lambas, D. G. 2004, MNRAS, 352, 1081
Anglés-Alcázar, D., Faucher-Giguère, C.-A., Kereš, D., et al. 2017, MNRAS, 470, 4698
Barnes, J. E., & Hernquist, L. 1996, ApJ, 471, 115
Barnes, J. E., & Hernquist, L. E. 1991, ApJL, 370, L65
Barton, E. J., Arnold, J. A., Zentner, A. R., Bullock, J. S., & Wechsler, R. H. 2007, ApJ, 671, 1538
Barton, E. J., Geller, M. J., & Kenyon, S. J. 2000, ApJ, 530, 660
Bassini, L., Feldmann, R., Gensior, J., et al. 2024, MNRAS, 532, L14
Behroozi, P. S., Wechsler, R. H., & Wu, H.-Y. 2013a, ApJ, 762, 109
Behroozi, P. S., Wechsler, R. H., Wu, H.-Y., et al. 2013b, ApJ, 763, 18
Bell, E. F., Phleps, S., Somerville, R. S., et al. 2006, ApJ, 652, 270

Bergvall, N., Marquart, T., Way, M. J., et al. 2016, A&A, 587, A72
Blumenthal, K. A., Moreno, J., Barnes, J. E., et al. 2020, MNRAS, 492, 2075
Bottrell, C., Yesuf, H. M., Popping, G., et al. 2024, MNRAS, 527, 6506
Cenci, E., Feldmann, R., Gensior, J., et al. 2024, MNRAS, 527, 7871
Colina, L., Arribas, S., & Monreal-Ibero, A. 2005, ApJ, 621, 725
Conselice, C. J., Bershady, M. A., Dickinson, M., & Papovich, C. 2003, AJ, 126, 1183
Cox, T. J., Jonsson, P., Primack, J. R., & Somerville, R. S. 2006, MNRAS, 373, 1013
Cox, T. J., Jonsson, P., Somerville, R. S., Primack, J. R., & Dekel, A. 2008, MNRAS, 384, 386
D'Onghia, E., Vogelsberger, M., Faucher-Giguère, C.-A., & Hernquist, L. 2010, ApJ, 725, 353
Ellison, S. L., Patton, D. R., Simard, L., & McConnachie, A. W. 2008, AJ, 135, 1877
Ellison, S. L., Patton, D. R., Simard, L., et al. 2010, MNRAS, 407, 1514
Ellison, S. L., Thorp, M. D., Lin, L., et al. 2020, MNRAS, 493, L39
Faucher-Giguère, C.-A. 2018, MNRAS, 473, 3717
Feldmann, R., Quataert, E., Hopkins, P. F., Faucher-Giguère, C.-A., & Kereš, D. 2017, MNRAS, 470, 1050
Fensch, J., Renaud, F., Bournaud, F., et al. 2017, MNRAS, 465, 1934
Gao, Y., & Solomon, P. M. 2004, ApJ, 606, 271
García-Burillo, S., Usero, A., Alonso-Herrero, A., et al. 2012, A&A, 539, A8
Garrison-Kimmel, S., Hopkins, P. F., Wetzel, A., et al. 2019, MNRAS, 487, 1380
Garrison-Kimmel, S., Wetzel, A., Bullock, J. S., et al. 2017, MNRAS, 471, 1709
Gurvich, A. B., Stern, J., Faucher-Giguère, C.-A., et al. 2023, MNRAS, 519, 2598
Hafen, Z., Stern, J., Bullock, J., et al. 2022, MNRAS, 514, 5056
Heiderman, A., Jogee, S., Marinova, I., et al. 2009, ApJ, 705, 1433
Hopkins, P. F. 2015, MNRAS, 450, 53
Hopkins, P. F., Cox, T. J., Hernquist, L., et al. 2013, MNRAS, 430, 1901
Hopkins, P. F., Croton, D., Bundy, K., et al. 2010, ApJ, 724, 915
Hopkins, P. F., Gurvich, A. B., Shen, X., et al. 2023, MNRAS, 525, 2241
Hopkins, P. F., & Hernquist, L. 2010, MNRAS, 402, 985
Hopkins, P. F., Kereš, D., Oñorbe, J., et al. 2014, MNRAS, 445, 581
Hopkins, P. F., Wetzel, A., Kereš, D., et al. 2018, MNRAS, 480, 800
Hung, C.-L., Sanders, D. B., Casey, C. M., et al. 2013, ApJ, 778, 129
Hunter, J. D. 2007, CSE, 9, 90
Jackson, R. A., Kaviraj, S., Martin, G., et al. 2022, MNRAS, 511, 607
Jog, C. J., & Solomon, P. M. 1992, ApJ, 387, 152
Keel, W. C., Kennicutt, R. C., Jr., Hummel, E., & van der Hulst, J. M. 1985, AJ, 90, 708
Kennicutt, R. C., Jr. 1983, ApJ, 272, 54
Kereš, D., Katz, N., Weinberg, D. H., & Davé, R. 2005, MNRAS, 363, 2
Knapen, J. H., & Cisternas, M. 2015, ApJL, 807, L16
Knapen, J. H., & James, P. A. 2009, ApJ, 698, 1437
Lackner, C. N., Silverman, J. D., Salvato, M., et al. 2014, AJ, 148, 137
Larson, R. B., & Tinsley, B. M. 1978, ApJ, 219, 46
Lofthouse, E. K., Kaviraj, S., Conselice, C. J., Mortlock, A., & Hartley, W. 2017, MNRAS, 465, 2895
Loken, C., Gruner, D., Groer, L., et al. 2010, JPhCS, 256, 012026
Luo, W., Yang, X., & Zhang, Y. 2014, ApJL, 789, L16
Ma, X., Hopkins, P. F., Faucher-Giguère, C.-A., et al. 2016, MNRAS, 456, 2140
Ma, X., Hopkins, P. F., Feldmann, R., et al. 2017, MNRAS, 466, 4780
Mantha, K. B., McIntosh, D. H., Brennan, R., et al. 2018, MNRAS, 475, 1549
Marszewski, A., Sun, G., Faucher-Giguère, C.-A., Hayward, C. C., & Feldmann, R. 2024, ApJL, 967, L41
Martin, G., Kaviraj, S., Devriendt, J. E. G., et al. 2017, MNRAS, 472, L50
McCluskey, F., Wetzel, A., Loebman, S. R., et al. 2024, MNRAS, 527, 6926
Mihos, J. C., & Hernquist, L. 1994, ApJL, 425, L13
Mihos, J. C., & Hernquist, L. 1996, ApJ, 464, 641
Montuori, M., Di Matteo, P., Lehnert, M. D., Combes, F., & Semelin, B. 2010, A&A, 518, A56
Moreno, J. 2012, MNRAS, 419, 411
Moreno, J., Bluck, A. F. L., Ellison, S. L., et al. 2013, MNRAS, 436, 1765
Moreno, J., Torrey, P., Ellison, S. L., et al. 2021, MNRAS, 503, 3113
Muratov, A. L., Kereš, D., Faucher-Giguère, C.-A., et al. 2015, MNRAS, 454, 2691
Nikolic, B., Cullen, H., & Alexander, P. 2004, MNRAS, 355, 874
Patton, D. R., Ellison, S. L., Simard, L., McConnachie, A. W., & Mendel, J. T. 2011, MNRAS, 412, 591
Pearson, W. J., Wang, L., Alpaslan, M., et al. 2019, A&A, 631, A51
Perret, V., Renaud, F., Epinat, B., et al. 2014, A&A, 562, A1
Ponce, M., van Zon, R., Northrup, S., et al. 2019, PEARC '19: Proc. of the Practice and Experience in Advanced Research Computing on Rise of the Machines (New York: ACM),
Renaud, F., Bournaud, F., Agertz, O., et al. 2019, A&A, 625, A65
Renaud, F., Bournaud, F., Kraljic, K., & Duc, P.-A. 2014, MNRAS, 442, L33
Robaina, A. R., Bell, E. F., Skelton, R. E., et al. 2009, ApJ, 704, 324
Robertson, B., Bullock, J. S., Cox, T. J., et al. 2006, ApJ, 645, 986
Rodighiero, G., Daddi, E., Baronchelli, I., et al. 2011, ApJL, 739, L40
Rodriguez-Gomez, V., Genel, S., Vogelsberger, M., et al. 2015, MNRAS, 449, 49
Rupke, D. S. N., Kewley, L. J., & Barnes, J. E. 2010, ApJL, 710, L156
Samuel, J., Wetzel, A., Tollerud, E., et al. 2020, MNRAS, 491, 1471
Sanders, D. B., Soifer, B. T., Elias, J. H., et al. 1988, ApJ, 325, 74
Schreiber, C., Pannella, M., Elbaz, D., et al. 2015, A&A, 575, A74
Scudder, J. M., Ellison, S. L., Momjian, E., et al. 2015, MNRAS, 449, 3719
Silva, A., Marchesini, D., Silverman, J. D., et al. 2018, ApJ, 868, 46
Sparre, M., Hayward, C. C., Feldmann, R., et al. 2017, MNRAS, 466, 88
Sparre, M., & Springel, V. 2016, MNRAS, 462, 2418
Stern, J., Faucher-Giguère, C.-A., Fielding, D., et al. 2021, ApJ, 911, 88
Sun, G., Faucher-Giguère, C.-A., Hayward, C. C., et al. 2023, ApJL, 955, L35
Tissera, P. B., Domínguez-Tenreiro, R., Scannapieco, C., & Sáiz, A. 2002, MNRAS, 333, 327
Toomre, A., & Toomre, J. 1972, ApJ, 178, 623
Torrey, P., Cox, T. J., Kewley, L., & Hernquist, L. 2012, ApJ, 746, 108
Turk, M. J., Smith, B. D., Oishi, J. S., et al. 2011, ApJS, 192, 9
van der Walt, S., Colbert, S. C., & Varoquaux, G. 2011, CSE, 13, 22
Veilleux, S., Kim, D. C., & Sanders, D. B. 2002, ApJS, 143, 315
Wetzel, A., Hayward, C. C., Sanderson, R. E., et al. 2023, ApJS, 265, 44
Wetzel, A. R., Hopkins, P. F., Kim, J. H., et al. 2016, ApJL, 827, L23
Woods, D. F., & Geller, M. J. 2007, AJ, 134, 527
Woods, D. F., Geller, M. J., & Barton, E. J. 2006, AJ, 132, 197
Woods, D. F., Geller, M. J., Kurtz, M. J., et al. 2010, AJ, 139, 1857
Yu, S., Bullock, J. S., Gurvich, A. B., et al. 2023, MNRAS, 523, 6220
Yu, S., Bullock, J. S., Klein, C., et al. 2021, MNRAS, 505, 889